

Numerical study of a direct current plasma sheath based on kinetic theory

Aleksey V. Vasenkov^{a)} and Bernie D. Shizgal^{b)}

Department of Chemistry, University of British Columbia, 2036 Main Mall, Vancouver, British Columbia V6T 1Z1, Canada

(Received 20 August 2001; accepted 29 October 2001)

A fully kinetic theory model was developed to study plasma properties of the sheath of a direct current glow discharge. This model includes a direct numerical solution of the Boltzmann equations for electron and ion distribution functions with a self-consistent electric field obtained from the Poisson equation. The calculated profiles of density, drift velocity, temperature, and electric potential were used to show the structure of the plasma sheath. The results of the direct numerical solution were compared with a particle-in-cell Monte Carlo simulation. It was also demonstrated that for a small Debye length to the ion mean-free path ratio, results obtained using the continuum sheath model, which includes two parameters, can be matched to the kinetic theory simulations.

© 2002 American Institute of Physics. [DOI: 10.1063/1.1432316]

I. INTRODUCTION

Much attention has been given recently to glow discharge plasmas of the type used for electronic material processing.¹ One of the central problems is to study the non-equilibrium transport of electron and ions in the region close to the electrode. This region is referred to as the sheath, and is not rigorously defined. Plasma properties change dramatically in the sheath region, and the electric field is not known *a priori* but must be found self-consistently. Although radio frequency (rf) discharge plasmas are usually used for material processing, we consider the plasma sheath of a direct current (dc) discharge in this study. An analysis of the dc sheath problem should be applicable to an rf sheath in the limit that the ion transit time multiplied by the rf frequency is small or large.^{1,2}

Our current goal is to present a detailed analysis of the behavior of a partially ionized plasma in contact with an electrode. We consider a one-dimensional (planar) sheath of a dc discharge such that the spatial dependence is only in the r axis measured from the electrode. We do not attempt to develop a model for the entire discharge. Instead, we introduce unequal fluxes of electrons and ions at the plasma-sheath boundary and focus on the nonequilibrium effects in the transport of electrons and ion in the sheath region.

Historically, sheath structure is described with simple hydrodynamic models which are based on the following two assumptions. First, the ionization in the sheath can be neglected and, second, electrons are considered to be at equilibrium and their number density is given by the Boltzmann relation $n(r) = n(0) \exp[e\phi(r)/kT_e]$, where $\phi(r)$ is the potential, e is the charge on an electron and T_e is the electron temperature.¹ In addition, it is often assumed that monoenergetic ions of mass M_i and temperature T_i enter the sheath region with velocity u_0 and $T_i \ll T_e$. The electric potential is

determined from the Poisson equation with the ion density given with conservation of ion density and momentum.³⁻⁶ If λ_D is the Debye length and L_i is the ion mean-free path, then this model is generally considered in the limit $\epsilon = \lambda_D/L_i \rightarrow 0$ and one finds that $u_0 \geq \sqrt{kT_e/m_i}$; that is, the speed of the ions entering the sheath region has to be greater than or equal to the ion sound speed. This is the usual Bohm criterion that has been discussed extensively.^{4,6-8} This hydrodynamic model cannot be rigorously valid in the region near the wall. The plasma sheath problem is a nonequilibrium system and the spatial and velocity distribution functions of the ions and electrons are not rigorously the Maxwell-Boltzmann distributions.

The main objective of this paper is to consider a kinetic theory treatment and determine the plasma properties from the solution of the ion and electron Boltzmann equations coupled to the Poisson equation for the self-consistent electric field. This is a formidable multidimensional problem for which the solution has been reported only in some cases. Quite often this solution is obtained on the condition that the spatial variations of plasma parameters are ignored and/or the spatial dependence of an electric field is imposed.⁹⁻¹⁵ In several studies hybrid models were reported which combine continuum and kinetic approaches (see, for example, Refs. 16-23). Here, the electric field is obtained from the hydrodynamic model, whereas a kinetic approach is used to calculate the nonequilibrium (high-energy) part of ion and/or electron velocity distribution functions. A promising convective scheme of the direct solution of the Boltzmann equation is described in Refs. 24-26. The authors show that this scheme is more efficient than the standard explicit finite difference scheme. Dalvie *et al.*²⁷ reported Monte Carlo (MC) simulations with a self-consistent electric field obtained from the solution of the Poisson equation. These authors performed MC simulations with the use of constant collision cross sections. The use of this unrealistic collisional model allows for a very simple MC algorithm. The present paper is a sequel to an early paper²⁸ where a detailed study of the spatial dependence of the nonequilibrium ion and electron distribution

^{a)}Permanent address: Institute of Thermophysics, Novosibirsk, 630090, Russia; electronic mail: vasenkov@theory.chem.ubc.ca

^{b)}Electronic mail: shizgal@theory.chem.ubc.ca URL: <http://www.chem.ubc.ca/personnel/faculty/shizgal/>

functions in the sheath region was reported. In this previous work, the range of validity of the Boltzmann relation for the spatial distribution of electrons was studied and discussed. In the present paper, we focus on the hydrodynamic variables such as density, drift velocity, and averaged energies expressed as temperatures derived from the nonequilibrium distribution functions.

In Sec. II, we present our kinetic theory model of the sheath. The direct numerical solution (DNS) of the Boltzmann equations for electron and ion distribution functions with a self-consistent electric field obtained from the Poisson equation is described in detail. Only a brief summary of our particle-in-cell Monte Carlo (PIC-MC) method is presented, as it was described previously in Ref. 28. Section III presents the results of calculations for the sheath region in a dc glow discharge in Ar.

II. SELF-CONSISTENT KINETIC THEORY OF A PLASMA SHEATH

A. Direct numerical solution

The self-consistent model of electron and ion transport in a boundary layer between the plasma and an electrode requires the solution of the Boltzmann equations for the distribution functions of electrons, $\tilde{f}_e(r, \mathbf{v}, t)$, and ions $\tilde{f}_i(r, \mathbf{v}, t)$, and coupled to the Poisson equation for the self-consistent field. We consider a one-dimensional discharge such that the spatial dependence is only in the r axis. We consider a system of electrons and ions dilutely dispersed in a background of atoms considered at equilibrium. The Boltzmann equations for the electron and ion distribution functions are given by

$$\frac{\partial \tilde{f}_e}{\partial t} + \mu v \frac{\partial \tilde{f}_e}{\partial r} - \mu \frac{e\tilde{E}}{m_e} \frac{\partial \tilde{f}_e}{\partial v} = n_g \tilde{J}_e[\tilde{f}_e], \quad (1)$$

$$\frac{\partial \tilde{f}_i}{\partial t} + \mu v \frac{\partial \tilde{f}_i}{\partial r} + \mu \frac{e\tilde{E}}{M_i} \frac{\partial \tilde{f}_i}{\partial v} = n_g \tilde{J}_i[\tilde{f}_i], \quad (2)$$

where $\mu = \cos \theta$, and θ is the angle relative to the r axis; m_e and M_i are the electron and ion masses, respectively; and n_g is the neutral gas density. We have written the time-dependent forms of the Boltzmann equations, although it is the steady distributions that are desired. The electric field, \tilde{E} , in (1) is determined from the Poisson equation

$$\frac{\partial \tilde{E}}{\partial r} = \frac{e}{\epsilon_0} (\tilde{n}_i - \tilde{n}_e), \quad (3)$$

where e is the electron charge and ϵ_0 is the vacuum permittivity. The electric field is derivable from the scalar potential, φ , that is

$$\tilde{E} = - \frac{\partial \tilde{\varphi}}{\partial r}, \quad (4)$$

where the steady electron and ion densities, $n_e(r)$ and ions $n_i(r)$, respectively, are determined by

$$\tilde{n}_e(r) = \int \tilde{f}_e(r, v, \mu) dv, \quad (5)$$

$$\tilde{n}_i(r) = \int \tilde{f}_i(r, v, \mu) dv. \quad (6)$$

We have suppressed the time variable as it is the steady distribution functions which are sought. The linear collision operator for electron-neutral interactions, \tilde{J}_e , is given by the Lorentz-Fokker-Planck form^{29,30}

$$\tilde{J}_e[\tilde{f}_e] = \frac{m_e}{M} \frac{1}{v^2} \frac{\partial}{\partial v} \left\{ \left[\sigma_m(v) v^4 \left(1 + \frac{kT_1}{m_e v} \frac{\partial}{\partial v} \right) \right] \tilde{f}_e(r, v, \mu) \right\} + \frac{\sigma_m(v) v}{2} \frac{\partial}{\partial \mu} \left\{ (1 - \mu^2) \frac{\partial}{\partial \mu} [\tilde{f}_e(r, v, \mu)] \right\}, \quad (7)$$

where $\sigma_m(v)$ is the momentum transfer cross section, M and T_1 are the atom mass and the temperature of the background medium, respectively. The first term in brace brackets in Eq. (7) is the isotropic portion of the operator whereas the second term is the anisotropic part which describes pitch-angle scattering.

We assume that the major process for ion-neutral collision is the charge-exchange process, for which the collision operator, \tilde{J}_i , is of the form

$$\tilde{J}_i[\tilde{f}_i(r, v, \mu)] = \tilde{f}_i^M(v) \int \tilde{f}_i(r, v', \mu) \sigma_{\text{ex}}(g) g dv' - \tilde{f}_i(r, v, \mu) \int \tilde{f}_i^M(v') \sigma_{\text{ex}}(g) g dv', \quad (8)$$

where $\sigma_{\text{ex}}(v)$ is the charge exchange cross section, $g = |\mathbf{v} - \mathbf{v}'|$ is the relative velocity. In (8), the Maxwellian distribution is defined by $\tilde{f}_i^M(v) = (M_i/2\pi kT_1)^{3/2} \times \exp(-M_i v^2/2kT_1)$. In the present paper, we have chosen a simple collisional operator based only on charge-exchange collisions within the linear trajectory approximation.^{31,32} The result is the collisional operator given by Eq. (8). For elastic collisions, the differential cross section, which is presently not available, should be calculated quantum mechanically from *ab initio* potentials.³³ The collision operator for these elastic collisions introduces additional complexities that will be considered in a future publication. When written explicitly in terms of spherical velocity components, the operator for charge-exchange collisions of ions with neutrals is given by

$$\begin{aligned} \tilde{J}_i[\tilde{f}_i] &= (M_i/2\pi kT_1)^{3/2} \exp(-M_i v^2/2kT_1) \\ &\times \int_0^\infty \int_{-1}^1 \int_0^{2\pi} \sigma_{\text{ex}}(g) g \tilde{f}_i(r, v', \mu) v'^2 dv' d\mu \\ &\times d\phi - (M_i/2\pi kT_1)^{3/2} \tilde{f}_i(r, v, \mu) \\ &\times \int_0^\infty \int_{-1}^1 \int_0^{2\pi} \sigma_{\text{ex}}(g) g \\ &\times \exp(-M_i v'^2/2kT_1) v'^2 dv' d\mu d\phi. \end{aligned} \quad (9)$$

We introduce the ion mean free path, $L_i = 1/n_g \sigma_i$, and the reference density given by $n_0 = j_0/D_a n_g \sigma_0$ with the flux $j_0 = 1 \text{ cm}^{-2} \text{ s}^{-1}$. Here, $\sigma_0 = 1 \text{ \AA}$, D_a is the ambipolar diffusion coefficient, and σ_i is the charge-exchange cross section

calculated at the energy corresponding to the ion temperature, T_i , chosen far from the electrode. We also introduce a dimensionless spatial variable defined as $x=r/L_i$ and dimensionless velocity variables for electrons, $p=v/v_e$, and ions, $P=v/v_i$, where $v_e=(2kT_e/m_e)^{1/2}$ and $v_i=(2kT_i/M_i)^{1/2}$. Similarly, we define dimensionless times for electrons and ions, $t_e=\tilde{t}v_e/L_i$, $t_i=\tilde{t}v_i/L_i$, respectively. The distribution functions, densities, collision operators and fields can thus be written in dimensionless form and we have that $f_e=\tilde{f}_e v_e^3/n_0$, $f_i=\tilde{f}_i v_i^3/n_0$, $n_e=\tilde{n}_e/n_0$, $n_i=\tilde{n}_i/n_0$, $J_e[f]=\tilde{J}_e[\tilde{f}]/(\sigma_i v_e)$, $J_i[f]=\tilde{J}_i[\tilde{f}]/(\sigma_i v_i)$, $E=e\tilde{E}L_i/kT_e$, $\varphi=e\tilde{\varphi}/kT_e$. With the transformation to these dimensionless variables, Eqs. (1)–(3) can be rewritten as the system of equations

$$\frac{\partial f_e}{\partial t_e} + \mu p \frac{\partial f_e}{\partial x} - \frac{\mu E}{2} \frac{\partial f_e}{\partial p} = J_e[f], \tag{10}$$

$$\frac{\partial f_i}{\partial t_i} + \mu P \frac{\partial f_i}{\partial x} + \frac{\mu E}{2} \frac{T_e}{T_i} \frac{\partial f_i}{\partial P} = J_i[f], \tag{11}$$

$$n_e(x) = \int f_e(p, x, \mu) d\mathbf{p}, \tag{12}$$

$$n_i(x) = \int f_i(P, x, \mu) d\mathbf{P}, \tag{13}$$

$$\frac{\partial E}{\partial x} = \varepsilon^{-2}(n_i - n_e), \tag{14}$$

$$E = -\frac{\partial \varphi}{\partial x}, \tag{15}$$

where $\varepsilon=\lambda_D/L_i$ and λ_D is the Debye length given by $\lambda_D=(\varepsilon_0 kT_e/n_0 e^2)^{1/2}$. The ratio of the electron temperature to ion temperature appears in (11) because T_i is used to introduce the dimensionless ion velocity, whereas the electric field is divided by T_e . The parameter ε controls the spatial variation of the electric field indirectly, owing to the coupling of the Poisson equation with the Boltzmann equations.

The steady distributions for both electrons and ions are determined from the time-dependent Eqs. (10) and (11), respectively. The time derivatives in Eqs. (10) and (11) are reduced to algebraic form with an explicit finite difference method, that is

$$f_e^{n+1} = f_e^n - B_e \Delta t_e, \tag{16}$$

$$f_i^{n+1} = f_i^n - B_i \Delta t_i, \tag{17}$$

where $n+1$ and n denote successive times separated by Δt . The quantities B_e and B_i are evaluated at time denoted by n , and are defined by

$$B_e = p \mu \frac{\partial f_e}{\partial x} - \frac{\mu E}{2} \frac{\partial f_e}{\partial p} - J_e[f_e], \tag{18}$$

$$B_i = P \mu \frac{\partial f_i}{\partial x} + \frac{\mu E}{2} \frac{T_e}{T_i} \frac{\partial f_i}{\partial P} - J_i[f_i]. \tag{19}$$

Equations (18) and (19) are discretized with a collocation method which employs Legendre quadrature points for both the μ and x variables, and the nonclassical speed quadrature points for p and P . The derivative operators in x , p , and P in

Eqs. (18) and (19) are replaced with their matrix representatives as discussed by Shizgal,³⁴ and Blackmore and Shizgal.³⁵ The discretization is based on a discrete matrix derivative operator, defined such that

$$\left. \frac{dF(x)}{dx} \right|_{x=x_i} = \sum_{j=1}^N D_{ij} F(x_j). \tag{20}$$

This algorithm permits the reduction to algebraic form of differential operators, as occurs explicitly in Eqs. (18) and (19). The electron collision operator in the form of a differential Fokker–Planck operator in Eq. (8) can also be written in terms of first- and second-order derivative operators.³⁰ Equation (18) is thus written in discrete form, as given by

$$\begin{aligned} B_e(x_k, p_n, \mu_l) &= p_n \mu_l \sum_{j=1}^{N_x} D_{kj}^L f_e(x_j, p_n, \mu_l) \\ &\quad - \frac{\mu_l E_k}{2} \sum_{j=1}^{N_p} D_{nj}^S f_e(x_k, p_j, \mu_l) - \frac{m_e}{M} \frac{1}{p_n^2} \sum_{j=1}^{N_p} D_{nj}^S \frac{\sigma_m(p_j)}{\sigma_i} \\ &\quad \times p_j^4 \left[f_e(x_k, p_j, \mu_l) + \frac{1}{2p_j} \sum_{i=1}^{N_p} D_{ji}^S f_e(x_k, p_i, \mu_l) \right] \\ &\quad - \frac{\sigma_m(p_n)}{2\sigma_i} \sum_{j=1}^{N_\mu} D_{lj}^L (1 - \mu_j^2) \sum_{i=1}^{N_\mu} D_{ji}^L f_e(x_k, p_n, \mu_i), \end{aligned} \tag{21}$$

where D_{kj}^L and D_{nj}^S are the derivative matrix operators for Legendre and speed quadratures, respectively. The quantities N_x , N_p , and N_μ are the number of discrete quadrature points in the x , p , and μ variables. The first two terms in Eq. (21) correspond to the derivative terms in Eq. (18). The third term involving the square brackets is the isotropic portion of the electron–atom collision operator, whereas the last term involving the derivatives in μ arise from the anisotropic part of the collision operator. The ion–neutral charge-exchange integral operator can be evaluated using the quadrature formula for the speed weight function.^{34,35} The discrete form of Eq. (19) follows similarly, except that the ion–neutral charge-exchange collision operator is an integral operator and evaluated with the speed quadrature formula, that is

$$\begin{aligned} B_i(x_k, P_n, \mu_l) &= P_n \mu_l \sum_{j=1}^{N_x} D_{kj}^L f_i(x_j, P_n, \mu_l) + \frac{\mu_l E_k}{2} \frac{T_e}{T_i} \\ &\quad \times \sum_{j=1}^{N_p} D_{nj}^S f_i(x_k, P_j, \mu_l) - \frac{2}{\pi^{3/2}} \exp(-P_n^2) \\ &\quad \times \sum_{j=1}^{N_p} w_j^S \exp(P_j^2) \sum_{i=1}^{N_\mu} \sum_{m=1}^{N_\mu} w_i^L w_m^L \\ &\quad \times \frac{V_{jnilm}}{(1 - \mu_m^2)} \frac{\sigma_{ex}(V)}{\sigma_i} f_i(x_k, P_j, \mu_i) + \frac{2}{\pi^{3/2}} f_i(x_k, P_n, \mu_l) \\ &\quad \times \sum_{j=1}^{N_p} \sum_{i=1}^{N_\mu} \sum_{m=1}^{N_\mu} w_j^S w_i^L w_m^L \frac{V_{jnilm}}{(1 - \mu_m^2)} \frac{\sigma_{ex}(V)}{\sigma_i}, \end{aligned} \tag{22}$$

where $V_{jniilm} = P_j^2 + P_n^2 - 2P_n P_j \mu_{ilm}$, $\mu_{ilm} = \mu_l \mu_i - [(1 - \mu_l^2)(1 - \mu_i^2)]^{1/2} \mu_m$. The electric field at the j th collocation position was found from a solution of the Poisson equation, given by

$$E(x_j) = \sum_k D_{kj}^{-1} \varepsilon^{-2} [n_i(x_j) - n_e(x_j)]. \quad (23)$$

The electric field as $x \rightarrow \infty$ is calculated from the requirement that the motion of electrons and ions is described by the ambipolar diffusion³⁶

$$E(x)|_{x \rightarrow \infty} = \frac{D_i - D_a}{D_i} \frac{1}{x},$$

where the ambipolar diffusion coefficient is given by³⁶

$$D_a = \frac{D_e \mu_i + D_i \mu_e}{\mu_e + \mu_i}.$$

Here, D_e, D_i and μ_e, μ_i are the electron and ion coefficients of diffusion and mobility, respectively.

The method of solution follows earlier treatments of the Milne problem.^{37,30,35} The distribution function, f_i^0 , and electron distribution function, f_e^0 , far from the boundary at $x=0$ are given by

$$\begin{aligned} f_e^0(x_k, p_n, \mu_l) &= f_i^0(x_k, p_n, \mu_l) \\ &= -j_0 / D_a f^M(p_n) [q_a + x_k - \mu_l U(p_n)], \end{aligned} \quad (24)$$

serve as asymptotic boundary conditions. The coefficient q_a is the extrapolation length.^{37,30} These distribution functions are the asymptotic forms consistent with the Chapman–Enskog-type solution of the diffusion of ions or electrons through the background neutral gas at equilibrium. The distribution functions are close to Maxwellian with a small perturbation owing to the finite drift of electrons and ions. The perturbation is of the form³⁷

$$\mu_l U(p_n) = \sum_{n=0}^N d_n \psi_{nl}(p_n, \mu_l),$$

where the basis functions $\psi_{nl}(p_n, \mu_l)$ are the Laguerre-spherical harmonic basis functions.

The extrapolation length q_a , and the expansion coefficients d_n (which describe ambipolar transport electrons and ions far away from the electrode) are calculated from the solution of the Boltzmann equation^{37,30} with the collision operator I equal to

$$I = \frac{T_e}{T_e + T_i} \left(J_e[f] + \frac{T_i}{T_e} J_i[f] \right). \quad (25)$$

This choice for the collision operator I reduces the system of equations (10)–(15) to one equation. The temperature factors in (25) are different because T_i and T_e are used to introduce the dimensionless velocities in Boltzmann equations for ion and electron distribution functions, respectively.

The numerical solution of the system of equations (16)–(23) is obtained as given by the iterations in Eqs. (16) and (17). The initial distribution functions for electrons and ions in this time-dependent approach to steady state are chosen

according to the distribution represented by Eq. (24). The algorithm includes cycles, each of which involves the direct numerical solution of the Boltzmann equations for electron and ion distribution functions, subject to the Marshak boundary conditions,³⁰ and the Poisson equation for the self-consistent electric field. The electron and ion distribution functions, at the time t_n , are given by Eqs. (18) and (19), respectively. The electric field, used in Eqs. (18) and (19), is calculated by solving Eq. (23), which employs the electron and ion densities obtained at t_{n-1} . This procedure is repeated until the steady-state solution of Eqs. (18) and (19) is obtained.

B. The stochastic simulation

A PIC simulation is a widely used alternative approach to the direct solution of the system of equations (1)–(3). In the PIC method, a group of electrons (or ions) is represented by a single simulation particle. It is usually assumed that this particle has only short-range interactions with a gas atom which correspond to collisions. The statistical Monte Carlo collision technique is used to simulate these collisions. In the PIC-MC method, each particle moves in the electric field according to Newton's law. The self-consistent field is calculated from the solution of the Poisson equation with the density of electrons and ions obtained from the particle simulation.

In this study, we use the PIC-MC algorithm to study the steady space- and energy-dependent ion and electron distributions in the sheath region. Our algorithm is previously outlined in Ref. 28; hence, only a brief outline is given. The algorithm includes a Monte Carlo simulation of charged particle transport in a self-consistent electric field calculated using the Poisson equation. In the simulation, ensembles of electrons and ions with Maxwellian speed distributions are incident on the gas medium of finite extent in the r direction. The simulation code follows the drift of electrons and ions through the series of real and null collisions. In the case of a null collision, a particle emerges with an unchanged velocity. Consideration of null collisions is required to provide the efficient simulation of charged particle transport in the electric field.^{38–40}

The core of our algorithm consists of three primary procedures: the simulation of collisions, indexing and cross-referencing of particles, and the simulation of particle motion. At the end of the third procedure, spatial distributions of electrons and ions are obtained using the spatial coordinates and velocity components of simulation particles

$$n_s(r) = \frac{\sum_k n_s^k(r, \mathbf{p})}{\Delta r}, \quad (26)$$

where the subscript s represents the kind of particles (e for electrons and i for ions); $n_s^k(r, \mathbf{p})$ is the space- and velocity-dependent distribution function. The summation in (26) is over all particles in the spatial interval Δr centered at r . The Poisson equation is solved with the Quadrature Discretization Method,^{34,35} which permits the reduction of the differential operator to the algebraic form. The details of solution

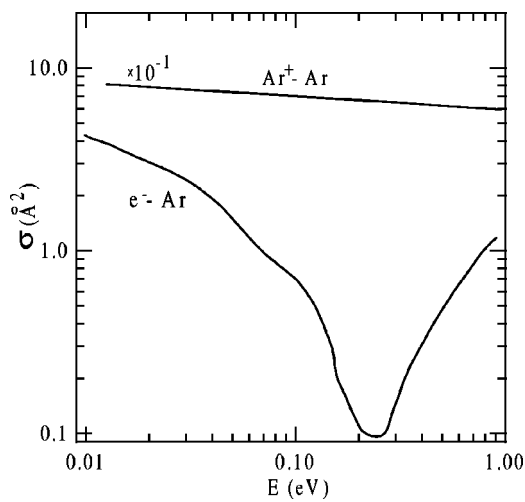


FIG. 1. Momentum transfer and charge-exchange cross sections for Ar.

are given in the previous subsection. These procedures are repeated until the steady-state distributions of ions and electrons are obtained.

The present model is used to determine the space- and energy-dependent ion and electron distribution functions

$$f_s(r, E) = \frac{\sum_k n_s^k(r, \mathbf{p})}{\Delta r \Delta E}, \quad (27)$$

where the summation is over all particles existing in the spatial interval Δr centered at r , and also in the energy interval ΔE centered at E .

III. RESULTS AND DISCUSSION

In this section, we present the plasma properties in the sheath region such as the electric potential, the electron and ion densities, the electron and ion drift velocities, and the electron and ion temperatures. In Fig. 1, we show the momentum transfer cross section for the electron-Ar elastic collisions taken from Ref. 41, and the charge-exchange cross section for $\text{Ar}^+ - \text{Ar}$ interactions obtained using the results from Ref. 42. We see that the charge-exchange cross section decreases slowly with an increase in energy, whereas the momentum transfer cross section exhibits a large Ramsauer-Townsend minima. The electron and ion velocity distribution functions far from the electrode are chosen to be Maxwellian distributions with temperatures $T_e^{(0)}$ and $T_i^{(0)}$, respectively. The calculations are performed for ion and background gas temperatures equal to 300 K. The electron temperature $T_e^{(0)}$ is chosen to be equal to either 300 or 3000 K.

In Sec. III A, we present the results for large and moderate ϵ . In this case, one has a relatively small charged particle density and, correspondingly, a relatively large (compare to the ion mean-free path) sheath width. The plasma parameters in this case are obtained with the PIC-MC method and the direct solution. Both these techniques are the common approaches in plasma discharge simulation. In Sec. III B, we present the results of PIC-MC simulation obtained for small ϵ and compare them with the results of simple fluid-type simulation. The latter type of simulation is also

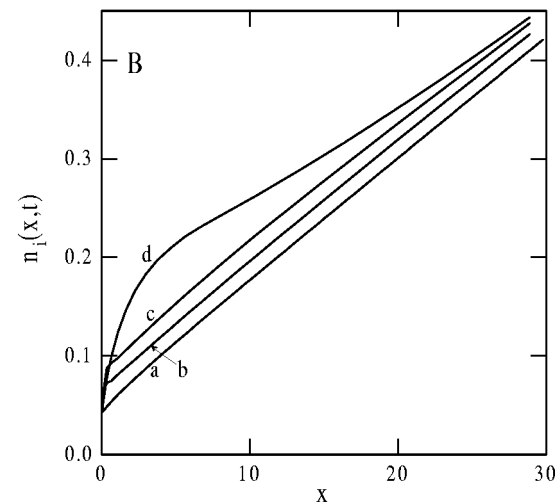
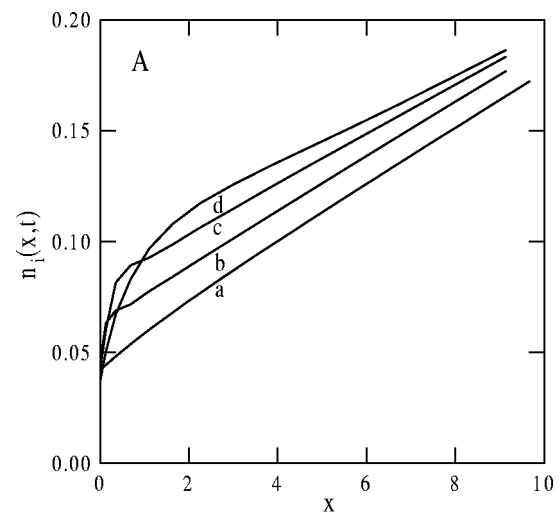


FIG. 2. Time evolution of the ion density, $n_i(x, t)$, in units of n_0 for ϵ equal to (A) 2.3 and (B) 7.7 for times t_i equal to (a) 0; (b) 0.08; (c) 0.23; (d) 0.77.

often used to model discharge plasmas. For the $\epsilon \rightarrow 0$ limit, we do not present the results of direct solution due to a few mathematical difficulties. These difficulties are related to the rapid variations of ion and electron distributions in the sheath, which has a width of about an ion mean-free path. In particular, we found that direct numerical solution requires a large number of points in velocity, angular and space variables. This implies very small time steps in Eqs. (16) and (17) and, correspondingly, an enormous number of iterations.

A. Large and moderate ratios of the Debye length to the ion mean-free path

The primary objectives of this work are the steady plasma parameters which are obtained with both the PIC-MC simulation and the direct solution of the Boltzmann equations. The time-dependent Boltzmann equations for electron and ion distribution functions Eqs. (16)–(19) are solved iteratively to obtain these steady-state plasma parameters. We employ typically 12 quadrature points for velocity, 21 and 60 Legendre quadrature points for angular and spatial variables, respectively. We first show the time evolution of

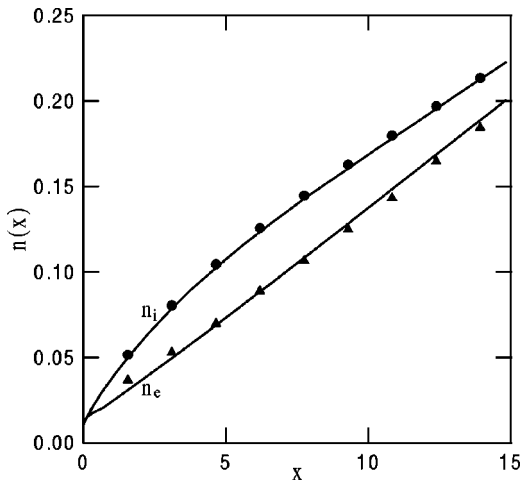


FIG. 3. Steady electron-density, $n_e(x)$, and ion-density, $n_i(x)$, profiles in units of n_0 for ϵ equal to 2.3 and $T_e^{(0)}$ equal to 300 K. Solid lines show the results of the direct solution, whereas PIC-MC simulations are represented by the symbols.

the spatial ion density profiles, $n_i(x, t)$, to the steady state profile. These profiles are shown as a function of position and time in Fig. 2(A) and Fig. 2(B) for ϵ equal to 2.3 and 7.7, respectively. The results of the direct solution are obtained for $T_e^{(0)} = 3000$ K. The initial density profile, shown by curve a in Fig. 2(A), is linear in the distance from the electrode owing to the choice of initial electron and ion distributions, Eq. (24). The density profile, calculated in $t = 0.08$ (curve b) is essentially nonlinear, especially near the electrode. The results, obtained for $t = 0.23$ (curve c) and $t = 0.77$ (curve d), show that the difference between the initial profile and $n_i(x, t)$ continues to grow with an increase in time. We can also see that curves (b–d) coincide very closely starting from x equal to approximately 20. This implies that $n_i(x, t)$ relaxes very fast to the time-independent distribution some distance away from the electrode. The time evolution of $n_i(x, t)$ for $\epsilon = 7.7$ is shown in Fig. 2(B). We see that the relaxation process in this case is slow in the beginning (curves a–c), but it becomes faster in the later part (curves c–d).

The spatial profiles of ion and electron densities obtained for $\epsilon = 2.3$ are shown in Fig. 3 and Fig. 4 for $T_e^{(0)}$ equal to 300 and 3000 K, respectively. The results of the direct numerical solution are shown by the curves, whereas the PIC-MC simulations are represented by the symbols. The ion and electron density are almost the same at the electrode, and are different some distance from the electrode. The difference between electron and ion densities for $T_e^{(0)} = 3000$ K (Fig. 4) is bigger than that shown in Fig. 3 in the case of $T_e^{(0)} = 300$ K. We show also in Fig. 4 the density profiles obtained with the Boltzmann relation

$$n_e(x) = n_0 \exp(\phi(x)/T_e), \tag{28}$$

where the electric potential, $\phi(x)$, is taken from the direct numerical solution. The electron density profile, obtained from Eq. (28) with $T_e(x)$ taken from the direct numerical solution, is shown by the dashed curve, while the dot-dashed curve represents Eq. (28) with the constant electric tempera-

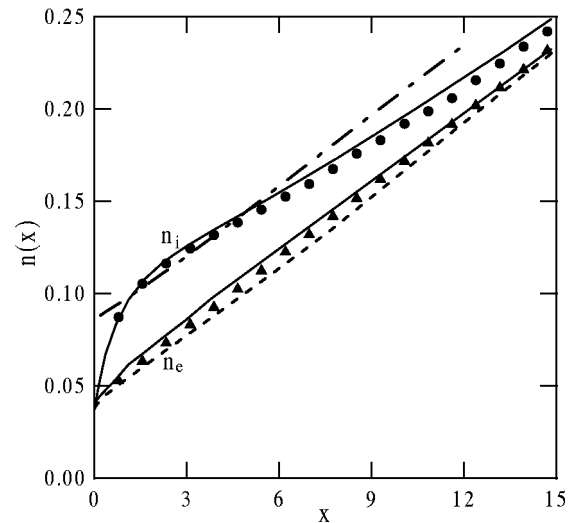


FIG. 4. Steady electron-density, $n_e(x)$, and ion-density, $n_i(x)$, profiles in units of n_0 for ϵ equal to 2.3 and $T_e^{(0)}$ equal to 3000 K. The dashed curve represents Eq. (28) with the calculated $T_e(x)$, while the dashed-dot curve is used to show the results obtained from Eq. (28) assuming the constant temperature.

ture equal to $T_e^{(0)}$. We see some difference between electron density obtained from the direct numerical solution and that calculated with the Boltzmann relation. This difference results from the departure of electron distribution function from the Maxwellian distribution. The ion and electron spatial density profiles obtained for $\epsilon = 0.46$ and $T_e^{(0)} = 3000$ K are shown in Fig. 5, now for x up to 12. We see that the boundary between sheath and plasma is closer to the electrode than it was in previous cases. The ion and electron density profiles are essentially nonlinear near the electrode. It is worth noting that the results of the direct simulation are not completely converged owing to a lack of the number of Legendre quadrature points for the spatial variable. We show also in Fig. 5 the electron density profiles calculated with the Boltzmann relation. The dashed curve represents Eq. (28)

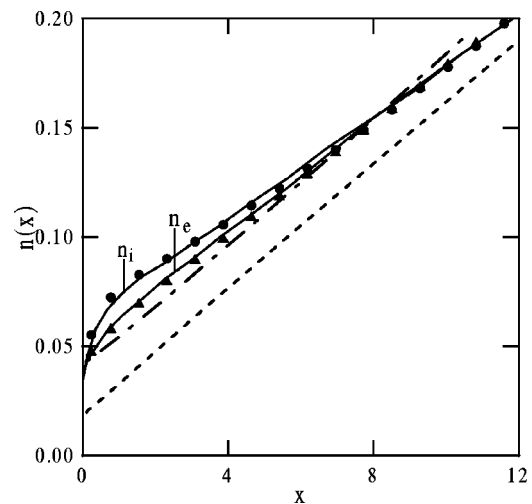


FIG. 5. Steady electron-density, $n_e(x)$, and ion-density, $n_i(x)$, profiles in units of n_0 for ϵ equal to 7.7 and $T_e^{(0)}$ equal to 3000 K. The dashed curve represents Eq. (28) with the calculated $T_e(x)$, while the dashed-dot curve is used to show the results obtained from Eq. (28) assuming the constant temperature.

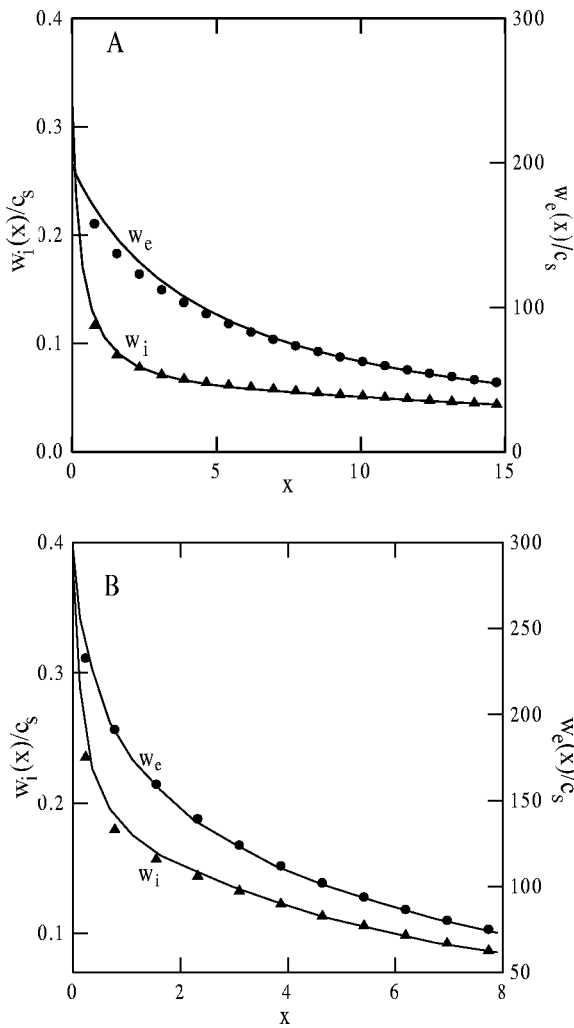


FIG. 6. Steady drift velocity profiles for ions, $w_i(x)/c_s$, and electrons $w_e(x)/c_s$, for ϵ equal to (A) 7.7 and (B) 0.46, $T_e^{(0)}$ equal to 3000 K.

with the calculated $T_e(x)$, while the dashed-dot curve is used to show the results obtained from Eq. (28) assuming the constant temperature. We see that the DNS results agree better with the dashed-dot curve rather than with the dashed curve.

The drift velocities of ions and electrons are shown in Figs. 6(A) and 6(B) for ϵ equal to 7.7 and 0.46, respectively. The electron temperature far from the electrode in both cases is equal to 3000 K. The results of the direct numerical solution are shown by the curves, whereas the PIC-MC simulations are represented by symbols. We see that the ion drift velocity in both cases does not reach the ion speed. Hence, Bohm's criterion is not satisfied in these cases owing to the small value of parameter ϵ . The ion and electron drift velocities shown in Fig. 6(B) increase faster with distance than in Fig. 6(A).

The spatial profiles of ion and electron temperatures obtained for $T_e^{(0)} = 3000$ K are shown in Figs. 7(A) and 7(B) for ϵ equal to 7.7 and 0.46, respectively. The ion temperature, shown in Fig. 7(A), is almost independent of x some distance away from the electrode and it decreases with x close to the electrode. In contrast, the ion temperature shown in Fig. 7(B) varies with x some distance away from the electrode and it is

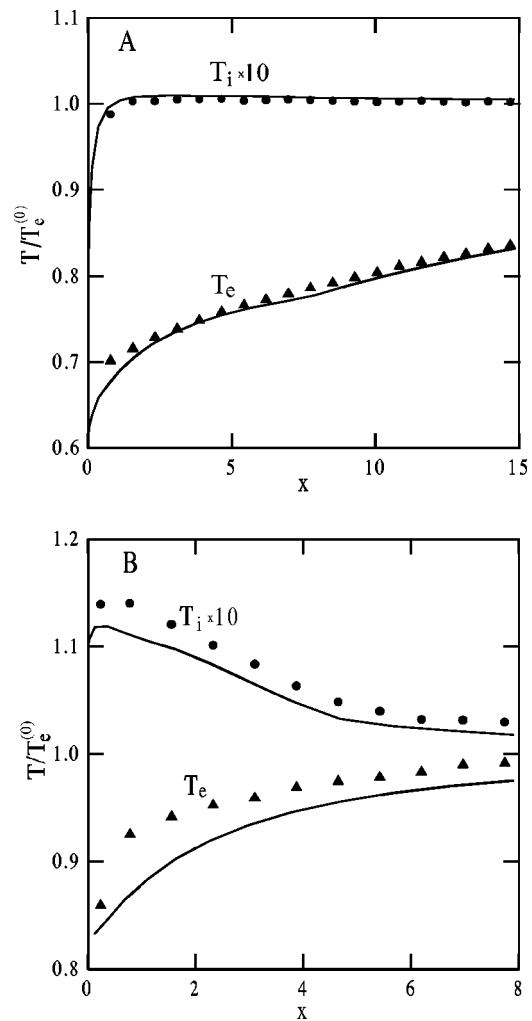


FIG. 7. Steady electron-temperature, $T_e(x)$, and ion-temperature, $T_i(x)$, profiles in units of $T_e^{(0)}$ for ϵ equal to (A) 7.7 and (B) 0.46, $T_e^{(0)}$ equal to 3000 K.

almost constant close to the electrode. A peak in ion temperature shown in Fig. 7(B) indicates that ions experience some heating in the sheath region owing to the drift in the self-consistent field. We will show later that the potential of this field in the sheath increases significantly with a decrease of ϵ . The electron temperature, shown in Figs. 7(A) and 7(B), decreases slowly with x . A similar result was obtained in the study of the nonequilibrium effects for electron transport near a boundary in the absence of an electric field.³⁰ The calculations also show that the electron temperature at the electrode grows slowly with the decrease of ϵ . It is also worth pointing out that the PIC-MC results are in better agreement with results of direct solution in the case of ϵ equal to 7.7 [Fig. 7(A)] rather than for ϵ equal to 0.46 [Fig. 7(B)]. This is probably due to the small number of quadrature points used in the direct numerical solution for moderate ϵ . An increase in the number of quadrature points would lead to the significant decrease of time step in Eq. (17), and, consequently, to a large number of iterations.

The electric potentials obtained for ϵ equal to 7.7 (curve a), 2.3 (curve b), and 0.46 (curve c) are shown in Fig. 8. The results of the PIC-MC simulations, which are represented by

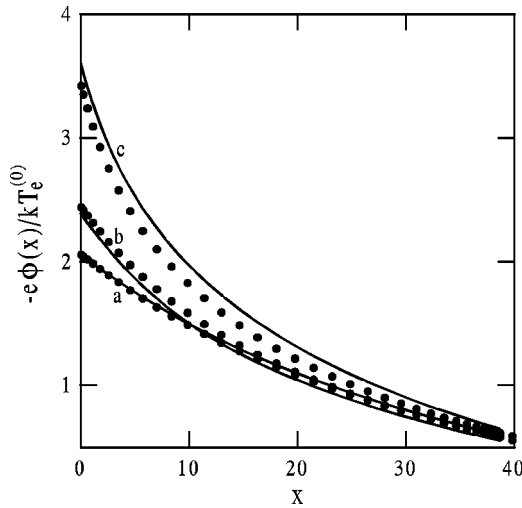


FIG. 8. Steady profiles of the potential, $e\phi(r)/kT_e^{(0)}$ for ϵ equal to (a) 7.7; (b) 2.3; (c) 0.46; $T_e^{(0)}$ equal to 3000 K.

the symbols, are in good agreement with the results of direct solution which is shown by the solid curves. We see that the results calculated for different ϵ are rather different close to the electrode; the value of the potential at the electrode slowly increases with the decrease of ϵ . Some distance away from the electrode, the spatial profiles of the potential converge to one curve which tends to a logarithmic potential shape.

B. Small ratios of the Debye length to the ion mean-free path: Comparison of continuum and kinetic approaches

In this subsection we present results obtained using the PIC-MC simulation for small, but finite ϵ . In this case, the ion temperature and the ion drift energy, $U_D(x) = Mw^2(x)/2$, change considerably within the sheath, as shown in Fig. 9. The simulation results are shown in the figure for $T_e^{(0)} = 3000$ K, $T_i^{(0)} = 300$ K, and $\epsilon = 0.008$. The

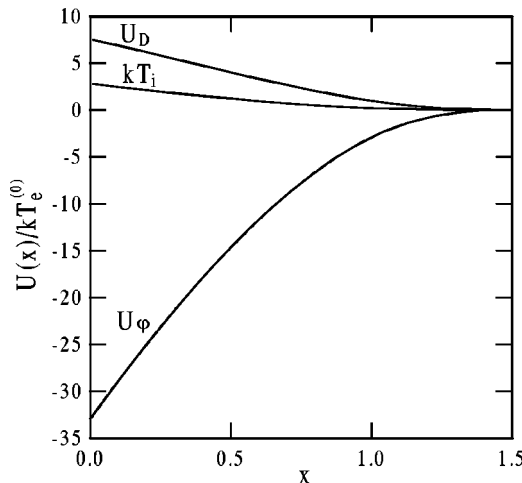


FIG. 9. Steady profiles of the ion temperature, $T_i(x)$, the ion drift energy, $U_D(x)$, and the ion potential energy $U_\phi(x)$ obtained using the PIC-MC method for ϵ equal to 0.008 and $T_e^{(0)}$ equal to 3000 K.

profile $U_\phi(x)$ represents the potential energy of the ions. We can see that both $kT_i(x)$ and $U_D(x)$ quickly grow with a decrease in x . This indicates that the ion motion in the sheath is essentially determined by the electric field. The ion drift energy increases faster than the ion temperature does. At the same time, it is important to point out that the sheath is collisional. Indeed, the decrease of ion potential energy with x is not compensated by an increase in ion thermal, $3kT_i(x)/2$ and drift, $U_D(x)$, energies. This implies that ions lose a considerable amount of energy through charge-exchange collisions with neutrals in the sheath.

Fluid-type simulations are computationally less intensive than kinetic theory models and are widely used to determine plasma properties in the sheath.^{3-6,43} These fluid-type simulations are criticized because the ion distribution function in the sheath is not close to the equilibrium Maxwellian distribution. This casts some doubts on the validity of plasma models based on the fluid-type equations, especially in the case of small but finite ϵ . In an attempt to clarify this point, we present a comparison of the PIC-MC simulations for small ϵ with results obtained using a simple continuum model.

The structure of static plasma sheath can be described using the system of equations which includes continuity and momentum transfer equations for the ions, Boltzmann relation for the electrons, and the Poisson equation.^{3,43} This system of equations can be reduced to the system of two coupled equations for the ion density and electric potential by neglecting the electron density in the Poisson equation which can be done for many plasma-sheath systems. The most important issue in the solution of this fluid-type system of equations is the plasma-sheath boundary conditions. The choice of these boundary conditions remains a matter of contention.^{3,6,43} We chose a plasma model proposed recently by Godyak and Sternberg⁴³ to perform a comparison between kinetic and continuum approaches. The model reported in Ref. 43 is easy to use since it does not require the introduction of the bulk plasma, presheath, and sheath regions but provides a smooth transition from the plasma to the sheath. These authors obtained the following system of equations for the plasma sheath in the case of a weakly ionized plasma:

$$\frac{\partial \phi}{\partial \xi} + \frac{2/\pi}{2/\pi + \alpha} n_i^{-3} \frac{\partial n_i}{\partial \xi} + \frac{\alpha}{2/\pi + \alpha} n_i^{-2} = 0, \tag{29}$$

$$\frac{\partial^2 \phi}{\partial \xi^2} = n_i(\xi), \tag{30}$$

where $\xi = x/\alpha$, $\alpha = \lambda_{Ds}/L_i$, and λ_{Ds} is the Debye length which is determined by plasma density and electron temperature at the plasma-sheath boundary.

The plasma model, presented by Godyak and Sternberg, includes two parameters: the electric potential at the electrode, ϕ_e , and collision parameter, α . Whereas the parameter ϕ_e is strictly defined, the definition of parameter α is rather ambiguous owing to the uncertainty in the definition of plasma-sheath boundary. We solved Eqs. (29) and (30) numerically for $\alpha = 0$ and $\alpha = 20.88\epsilon$. The latter parameter α was chosen to fit the shape of potential determined by Eqs.

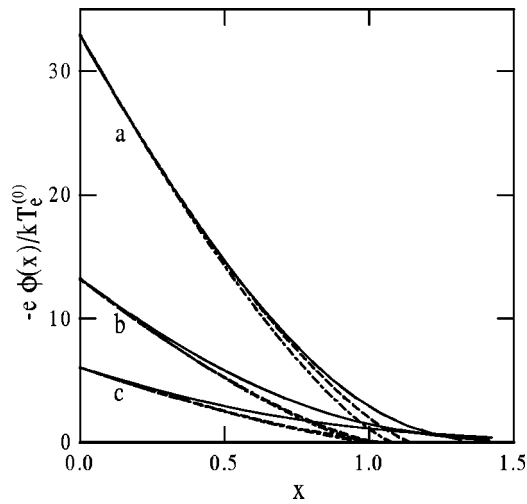


FIG. 10. Electric potential profile, $e\phi(r)/kT_e^{(0)}$ vs x for $\epsilon = 0.008$ (curve a), $\epsilon = 0.014$ (curve b), $\epsilon = 0.024$ (curve c). Solid lines represent PIC-MC calculations, whereas dashed and dot-dashed lines show the results of continuum sheath model (Ref. 43) for $\alpha = 20.88\epsilon$ and $\alpha = 0$, respectively.

(29) and (30) to that obtained from the PIC-MC simulation for $\epsilon = 0.008$. The value of the electric potential at the electrode was also taken from our PIC-MC calculations. The electric potential obtained as the result of the solution of Eqs.

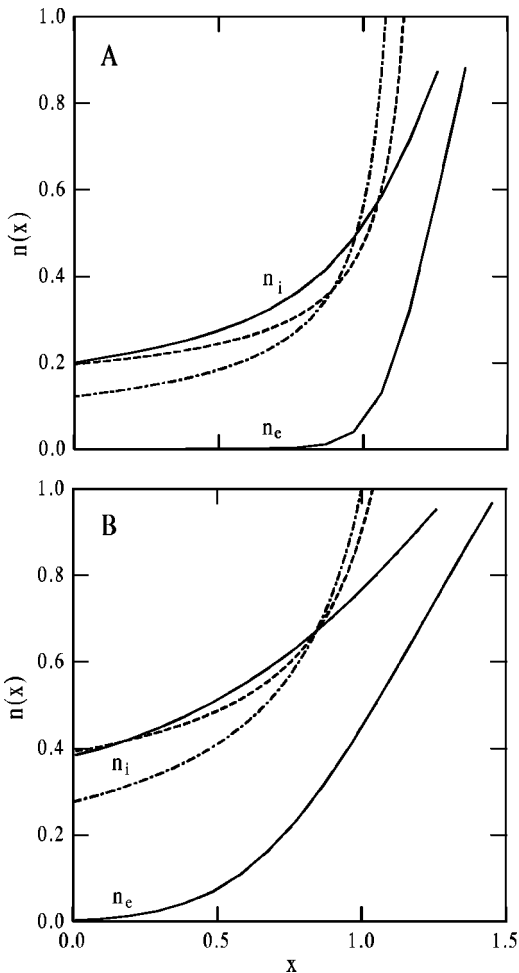


FIG. 11. Steady profiles of electron and ion densities vs x for (A) $\epsilon = 0.008$ and (B) $\epsilon = 0.024$. Designations are the same as in Fig. 10.

(1) and (2) is compared with the PIC-MC calculations in Fig. 10 for $\epsilon = 0.008$, (curve a); $\epsilon = 0.014$ (curve b); $\epsilon = 0.024$ (curve c). Solid lines represent PIC-MC calculations, whereas dashed and dot-dashed lines show the results of continuum sheath model for $\alpha = 20.88\epsilon$ and $\alpha = 0$, respectively. As one can see from Fig. 10, the results obtained with the continuum sheath model are not affected very much by the collisional parameter α .

The ion densities calculated with a PIC-MC simulation are compared with the results obtained using the continuum sheath model in Fig. 11(A) and Fig. 11(B) for $\epsilon = 0.008$, $\epsilon = 0.024$, respectively. Solid lines represent PIC-MC calculations, whereas dashed and dot-dashed lines show the results of continuum sheath model for $\alpha = 20.88\epsilon$ and $\alpha = 0$, respectively. We see that the ion density profile obtained using a fluid-type approach depends weakly on the collisional parameter α . Results obtained for $\alpha = 0$ underestimate the ion density profile calculated using the kinetic simulation, whereas results obtained for $\alpha = 20.88\epsilon$ are in agreement with the PIC-MC calculations.

IV. SUMMARY

A direct numerical solution of the time-dependent Boltzmann equations for the distribution functions of electrons and ions, coupled to the Poisson equation for the self-consistent electric field, was developed to study the plasma properties in the sheath of a dc glow discharge.

The steady profiles for electric potential, ion and electron densities, ion and electron temperatures, and ion and electron drift velocities were obtained with the direct numerical solution and compared with particle-in-cell Monte Carlo results for large and moderate ϵ . It was also demonstrated that for small ϵ , results obtained using a continuum sheath model can be matched to the kinetic theory simulations choosing appropriate values for the potential at the electrode and a collisional parameter. Both these parameters are not known *a priori*, but can be obtained using other results such as kinetic simulations or experimental data.

ACKNOWLEDGMENT

Acknowledgment is made to the Donors of the Petroleum Research Fund, administered by the American Chemical Society, for support of this research (PRF No. 34689-AC6).

¹M. A. Lieberman and A. J. Lichtenberg, *Principles of Plasma Discharges and Materials Processing* (Wiley, New York, 1994).
²Y. P. Raizer, *Gas Discharge Physics* (Springer, New York, 1991).
³K-U. Riemann, *J. Phys. D* **24**, 493 (1991).
⁴K-U. Riemann, *Phys. Plasmas* **4**, 4158 (1997).
⁵N. Sternberg and V. A. Godyak, *Physica D* **97**, 498 (1996).
⁶R. N. Franklin and J. Snell, *Phys. Plasmas* **8**, 643 (2001).
⁷H.-B. Valentini, *Phys. Plasmas* **3**, 4754 (1996).
⁸K-U. Riemann and P. Meyer, *Phys. Plasmas* **3**, 4751 (1996).
⁹P. Segur and R. Keller, *J. Comput. Phys.* **24**, 43 (1977).
¹⁰J. P. Boeuf and E. Marode, *J. Phys. D* **15**, 2169 (1982).
¹¹H. Itoh, N. Ikuta, and K. Toyota, *J. Phys. D* **16**, 293 (1983).
¹²T. N. An, E. Marodem, and P. C. Johnson, *J. Phys. D* **10**, 2317 (1977).
¹³R. J. Carman and A. Maitland, *J. Phys. D* **20**, 1021 (1987).
¹⁴R. J. Carman, *J. Phys. D* **22**, 55 (1989).

- ¹⁵S. Hashiguchi and M. Hasikuni, *Jpn. J. Appl. Phys.* **27**, 1010 (1988).
- ¹⁶T. J. Sommerer and M. J. Kushner, *J. Appl. Phys.* **71**, 1654 (1992).
- ¹⁷Ph. Belenquer and J.-P. Boeuf, *Phys. Rev. A* **41**, 4447 (1990).
- ¹⁸J.-P. Boeuf and L. C. Pitchford, *IEEE Trans. Plasma Sci.* **19**, 286 (1991).
- ¹⁹N. Sato and H. Tagashira, *IEEE Trans. Plasma Sci.* **19**, 102 (1991).
- ²⁰M. Surenda, D. B. Graves, and G. M. Jellum, *Phys. Rev. A* **41**, 1112 (1990).
- ²¹K. H. Schoenbach, H. Chen, and G. Schaefer, *J. Appl. Phys.* **67**, 154 (1990).
- ²²R. K. Porteous and D. B. Graves, *IEEE Trans. Plasma Sci.* **19**, 204 (1991).
- ²³M. Surenda, D. B. Graves, and L. S. Plano, *J. Appl. Phys.* **71**, 5189 (1992).
- ²⁴W. H. G. Hitchon, D. J. Koch, and J. B. Adams, *J. Comput. Phys.* **83**, 79 (1989).
- ²⁵T. J. Sommerer, W. N. G. Hitchon, R. E. P. Harvey, and J. E. Lawler, *Phys. Rev. A* **43**, 4452 (1991).
- ²⁶G. J. Parker and W. N. G. Hitchon, *Jpn. J. Appl. Phys.* **36**, 4799 (1997).
- ²⁷M. Dalvie, S. Hamaguchi, and R. T. Farouki, *Phys. Rev. A* **46**, 1066 (1992).
- ²⁸A. V. Vasenkov and B. D. Shizgal, *Phys. Rev. E* (in press).
- ²⁹A. Gilardini, *Low Energy Electron Collisions in Gases: Swarm and Plasma Methods Applied to their Study* (Wiley, New York, 1972).
- ³⁰A. V. Vasenkov and B. D. Shizgal, *Phys. Rev. E* **63**, 016401 (2001).
- ³¹T. Tokonami and T. Makabe, *J. Appl. Phys.* **72**, 3323 (1992).
- ³²D. Rapp and W. E. Francis, *J. Chem. Phys.* **37**, 2631 (1962).
- ³³H. R. Skullerud, T. H. Lovaas, and K. Tsurugida, *J. Phys. B* **32**, 4509 (1999).
- ³⁴B. Shizgal, *J. Comput. Phys.* **41**, 309 (1981).
- ³⁵R. Blackmore and B. Shizgal, *Phys. Rev. A* **31**, 1855 (1985).
- ³⁶M. Mitchner and C. H. Kruger, *Partially Ionized Gases* (Wiley, New York, 1973).
- ³⁷J. M. Lindenfeld and B. Shizgal, *Phys. Rev. A* **27**, 1657 (1983).
- ³⁸H. Skullerud, *J. Phys. B* **6**, 728 (1973).
- ³⁹S. L. Lin and J. N. Bardsley, *J. Chem. Phys.* **66**, 435 (1977).
- ⁴⁰M. J. Brennan, *IEEE Trans. Plasma Sci.* **19**, 256 (1991).
- ⁴¹M. Suzuki, T. Tanigushi, and H. Tagashira, *J. Phys. D* **23**, 842 (1990).
- ⁴²A. V. Phelps, *J. Phys. Chem. Ref. Data* **20**, 557 (1991).
- ⁴³V. A. Godyak and N. Sternberg, *IEEE Trans. Plasma Phys.* **18**, 159 (1990).